

Re-evaluation of ortho-para-dependence of self pressure-broadening in the $\nu_1 + \nu_3$ band of acetylene

Eisen C. Gross,^{1, a)} Kimberly A. Tsang,^{1, b)} and Trevor J. Sears^{1, c)}

Chemistry Department, Stony Brook University, Stony Brook, NY 11794-3400, USA

(Dated: 28 May 2022)

Optical frequency comb-referenced measurements of self pressure-broadened line profiles of the R(8) to R(13) lines in the $\nu_1 + \nu_3$ combination band of acetylene near $1.52\mu\text{m}$ are reported. The analysis of the data found no evidence for a previously reported [Iwakuni et al. *Phys. Rev. Letts.* **117**, 143902(5) 2016] systematic alternation in self pressure-broadened line widths with the nuclear spin state of the molecule. The present work brought out the need for the use of an accurate line profile model and a careful accounting for weak background absorptions due to hot-band and lower abundance isotopomer lines. The data were adequately fit using the quadratic speed-dependent Voigt profile model, neglecting the small speed-dependent shift. Parameters describing the most probable and speed-dependent pressure-broadening, most probable shift, and the line strength were determined for each line. Detailed modeling of the results of Iwakuni et al. showed that their neglect of collisional narrowing due to the speed-dependent broadening term, combined with the strongly absorbing data recorded and analyzed in transmission mode were likely the reasons for their results.

^{a)}Electronic mail: eisen.gross@stonybrook.edu

^{b)}Electronic mail: ktsang@estee.com; Now at: Estee Lauder Inc., Melville, NY 11747, USA

^{c)}Electronic mail: trevor.sears@stonybrook.edu

I. INTRODUCTION

The absorption spectra of molecules in a gaseous sample are broadened by a combination of the Doppler effect due to the Maxwell-Boltzmann distribution of velocities, and the lifetimes of the levels involved in the spectroscopic transition. For spectra in the infrared region, the natural lifetimes are normally very long and coherence lifetimes are limited by intermolecular collisions that alter the molecular velocity, the orientation of the molecule, or cause the molecule to transition to another quantum state entirely. As sample pressures are increased, so are the collision rates, and the widths of the Doppler-limited lines observed at low pressures are found to broaden and the line shape function changes. Understanding the variation of the shapes and widths of spectral lines as a function of pressure and composition is critical for remote sensing and other analytical applications and much effort has been expended in the measurement, calculation and modeling of observed line profiles.¹⁻⁵

Given our understanding of the phenomenon, it was therefore a surprise when, in 2016, Iwakuni et al.⁶ measured the well-studied $\nu_1 + \nu_3$ vibrational combination band of acetylene using a new instrument based on a dual frequency-comb⁷⁻¹² spectrometer and reported a large ($\approx 10\%$) alternation in the measured self pressure-broadening coefficients with rotational quantum number. Transitions involving acetylene molecules in the *ortho*- nuclear spin arrangement apparently showed a greater self pressure-broadening than *para*- ones. In the ground state of acetylene, *ortho*- nuclear spin symmetry is associated with odd rotational quantum number (J) levels, while *para*- are associated with even J levels, hence correlating with the alternation in line widths with rotational quantum number in the spectrum.

The observations were explained by the following arguments. Since the *ortho*- spin arrangement is statistically favored 3:1 to the *para*- one, *ortho*- *ortho*- collisions are more probable than *para*- *para*- ones, so that efficient resonant collisional energy transfer processes are more probable among *ortho*- molecules than *para*- ones. If the collisions that cause broadening are dominated by resonant energy transfer ones, then $\Delta J = \pm 2$ rotational energy transfer between molecules with common nuclear spin symmetry will be more efficient than other inelastic interactions. Having a light molecule where the rotational intervals are large compared to translational energies helps to see the effect because the $|\Delta J| = 2$

resonant collisions, become more probable than inelastic ones for large rotational energy spacings. The general idea was first described by Anderson in 1949.¹³ It is well documented in gaseous H₂, from rotational Raman spectra,^{14–16} but H₂ is a special case due to its huge rotational energy level spacings. There have been reports of analogous effects in HCl^{17–19} where the rotational energy spacings are also large, resulting in a peak in the pressure-broadening coefficient at low- J , and an oscillatory behavior in broadening at high- J . In HCN, the observed self pressure-broadening coefficient^{20–22} peaks at rotational levels at the maximum of the Maxwell-Boltzmann distribution, a fact explained by resonant rotational energy transfer processes dominating the collisional broadening. However there had been no observation of the effect in acetylene which does not possess a dipole moment and whose quadrupole moment is small.

The reported effects⁶ are comparable to or greater than the limits of the precision of data recorded using conventional Fourier Transform Infrared (FTIR) spectrometers, and so it was surprising that previous experimental measurements and analyses had missed the differences. The report was immediately controversial and theoretical calculations and analysis by Lehmann²³ suggested that effects of quadrupole-induced $|\Delta J| = 2$ resonant energy transfer could not explain the size of the measured differences. Separately, Hartmann and Tran²⁴ suggested that the use of an approximate Voigt profile (VP) model in the original analysis was at fault because fits of the measured transmission spectra were made, and the more strongly absorbing *ortho*- lines lead to systematically increased apparent widths compared to the less strongly absorbing *para*- lines due to the model deficiencies. The authors of the original work rebutted these arguments,²⁵ but no experimental study has yet been reported to confirm or deny the experimental results or to investigate the effects of using more accurate line profile models on precise experimental data.

In this work, we report measurements of the $R(8)$ to $R(13)$ rotational lines in the $\nu_1 + \nu_3$ band of pure acetylene gas in question. These lines showed the strongest *ortho*- *para*-pressure-broadening differences in the original report.⁶ The data were all recorded at (measured) ambient temperatures (295 to 300K) and over a pressure range from 0.14 to 7 kPa (1 to 52 torr). Measurements were made with an extended cavity diode laser (ECDL) locked to a component of an optical frequency comb (OFC) resulting in absolute frequencies and

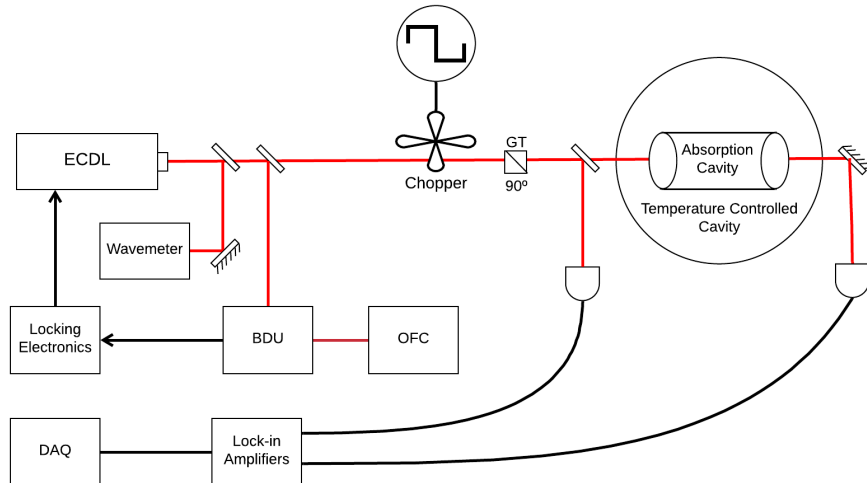
long-term optical frequency stability good to a few parts in 10^{11} . The pressure data for a given rotation-vibration line were analyzed in a multispectrum fit to extract line profile parameters. Several line profile models, derived from the Hartmann-Tran profile,^{26,27} were considered for use in the analysis, and the quadratic speed-dependent Voigt profile (QSDVP) model neglecting the speed-dependent shift (δ_2) was chosen based on its ability to reproduce the data using a minimal number of parameters. See also Atkins and Hodges²⁸ for a discussion of line profile choices for the analysis of experimental data. We found it necessary to account for the presence of weak underlying hot band and lower abundance isotopomer lines that affect the observed baselines and can distort line profiles of the spectra, but our analysis of the data showed no evidence for a systematic *ortho-para*- variation in pressure-broadening. Extensive modeling of synthetic data shows the most likely explanation for the original observations is that suggested by Hartmann and Tran.²⁴ The neglect of collisional narrowing in the Voigt line profile model used in the transmission representation and the large peak absorbances in the original work caused a systematic over-estimate of widths for the stronger absorbing *ortho*- lines even at pressures where collisional narrowing is small.

II. EXPERIMENTAL DETAILS

A. Probe laser and data acquisition

A tunable ECDL (Sacher Lasertechnik TEC 500) centered at 1550 nm was driven at 200.5 mA using an ILX Lightwave current supply. The output beam was passed through an optical isolator and split into two. The first beam containing 50% of the power was coupled into a fiber optic cable and directed to the beat detection unit (BDU) associated with a Menlo Systems FC-1500 OFC and described below. The second 50% of power was split again with 4% of it coupled into a fiber optic cable to a wavemeter (Bristol Instruments model 621B) for wavelength measurement. The remaining beam was scaled in size down one-third using a telescope and its spatial mode cleaned up before passing through an optical chopper (Scitec, 350CD) operated at ≈ 1650 Hz. Finally, the beam was split again using a 50:50 polarizing beamsplitter, creating two beam paths for sample and reference

FIG. 1. A simplified diagram of the experimental layout.



detectors. A Glan-Taylor prism was used before this final split to reduce the optical power and maintain a linear response of the detectors that are described in detail below. Typical continuous optical power at each of the detectors was estimated to be 0.07 mW under the conditions of the measurements.

The absorption cell used was a 1.085 cm cell machined from solid copper with indium sealed CaF_2 windows that was used previously.^{29,30} It was held inside a metal vacuum chamber equipped with wedged silica windows. The vacuum chamber incorporated a temperature-controlled mounting assembly giving a convenient way to monitor the cell temperature, while also providing temperature stabilization and gas leak prevention. To compensate for the two sets of windows in the sample beam, the reference beam was directed through a second cell (open to the air) and a variable neutral density filter to maintain equal optical power levels at the two detectors in the absence of any absorbing sample.

Finally, the sample and reference beams were focused onto a matched pair of detectors to provide sample transmission, I_t , and reference, I_0 signals. The two detectors were based on Hamamatsu InGaAs photodiodes (model G8605-11), with a negative-biased preamplifying circuit using an AD6202 op-amp. Their output signals were analyzed by two lock-in amplifiers (SRS, model SR830) controlled by LabView code over a GPIB bus, with the lock-in reference frequency provided by the chopper controller. The time constant used

for the lock-in amplifiers was 100 ms. The SRS SR830 amplifier uses a 24 bit Motorola DSP56001 chip clocked at 30 MHz so the Nyquist frequency is about half this, corresponding to a digitization time of $0.06 \mu\text{sec}$. A 160 mV signal from the detector was typical for a non-absorbing point, and the neutral density filter was used to ensure the detectors' outputs matched at the beginning of each scan.

A sample of purified acetylene gas was loaded into the absorption cell from a gas handling manifold to the desired pressure, and the cell was closed to the gas manifold and the pressure recorded. The manifold was evacuated using a turbomolecular pump. An MKS-398HD pressure gauge was used for all sample pressure measurements. Its absolute calibration was checked using a new MKS 902B-11010 piezoelectric transducer, and the maximum measurement error was found to be 0.24%. For a given sample pressure, data were recorded for the lines (R(8) to R(13)) in the vibrational band by scanning the down-mixed repetition rate frequency of the OFC. For the lowest two sets of pressures one scan of 12 kHz at 50 Hz increments resulted in a 2.1 GHz wide optical spectrum that was sufficient. However most data were recorded using two consecutive scans, resulting in 4.2 GHz wide spectra. This ensured an adequate amount of baseline was recorded for stable line profile fitting. Once all the lines for a given pressure were recorded, the manifold was closed to the pumping, the cell re-opened to it, and a second pressure measurement made. The known relative volumes of the cell and manifold allowed any cell leakage during the measurements to be checked and no changes outside the gauge error limits were detected during the measurements. Experimental conditions for the recorded lines are listed in table I.

TABLE I. Pressures used for the measurements, in kilo-pascals and torr.

Pressure		Lines
kPa	torr	Measured
7.0099	52.579	all lines
4.1394	31.048	R(9), R(11), R(13)
4.0045	30.036	R(8), R(10), R(12)
2.2035	16.528	all lines
1.091	8.184	all lines
0.6393	4.795	all lines
0.1384	1.038	all lines

B. Optical frequency comb

A K+K GPS receiver provided the 10 MHz laboratory clock reference, which was used for all frequencies needed for the experiment. The Menlo Systems FC-1500 OFC used in these measurements is based on a mode-locked Erbium fiber laser and has an extended output from 1050 to 2100 nm.

The ECDL was locked to the OFC via the BDU to improve its frequency precision and accuracy to the order of 10 ppt. The locking method relied on three consecutive feedback loops. The OFC repetition rate, f_r was measured by a photodiode, at the fiber laser output. This frequency was multiplied by 4 and mixed with a stable 980 MHz oscillator to produce a signal at about 20 MHz. A user-defined frequency from a SRS SG380 signal generator was mixed with this and generated a difference error signal for a digital phase-locked loop (PLL) that drove a piezoelectric translator (PZT) adjusting the cavity length of the fiber laser, and locking the repetition rate. The offset beat, f_o was measured using the $f-2f$ detection method,^{8,31} and in a similar way to the repetition rate, an error signal was generated with a fixed 20 MHz signal, and used to drive the pump laser to adjust the comb laser carrier envelope phase and therefore the offset. The output of the phase-locked OFC was directed to the BDU, where it was overlapped with a beam from the ECDL. The two beams were power balanced at the detector using polarized optics. The first-order diffraction beam from a grating angled to center the ECDL frequency was focused onto a detector, and its bandpass-filtered output was mixed with a reference 30 MHz frequency, to generate an error signal which drove the PZT of the ECDL cavity to maintain lock to the chosen comb component. The exact error frequency and its Allan variance was measured using a SRS SR620 frequency counter.

III. ANALYSIS

A. Line Modeling

Global fits of the sets of data corresponding to the same vibration-rotational transition at varying pressures (in table I) were performed. A suite of Python programs, described

and available as Supplementary Data for this paper, were written to read the data files, collate files by transition, fit the data to a normalized line shape function, and present the resulting line profile parameters. The analysis code could fit both the raw transmittance data or convert the data to absorbance, by taking the logarithm, before fitting.

Power transmittance, t , is usually defined as:

$$t(\tilde{\nu}) = \frac{I_t(\tilde{\nu})}{I_0(\tilde{\nu})} \quad (1)$$

where $\tilde{\nu}$ is the wavenumber (cm^{-1}) frequency of light, I_t is the intensity of a beam transmitted through a sample gas and I_0 is the initial beam intensity. According to the Beer-Lambert law, transmittance can be expressed as:

$$t(\tilde{\nu}) = e^{-\text{Amp} \times g(\tilde{\nu} - \tilde{\nu}_0)} \quad (2)$$

$g(\tilde{\nu} - \tilde{\nu}_0)$ is the area normalized line profile function for the molecular absorption centered around zero, and with:

$$\text{Amp} = S_{\tilde{\nu}}^N(T) \times N \times l_{\text{path}} \quad (3)$$

l_{path} is the optical pathlength in centimeters, and N is the number density of the gas, calculated by assuming the ideal gas law, such that $N = p/(k_B T)$, in units of molecules per cm^3 , with p the pressure, k_B the Boltzmann constant, and T the temperature. $S_{\tilde{\nu}}^N(T)$ is the spectral line strength at temperature T , and has units $\frac{\text{cm}^{-1}}{\text{molecules} \cdot \text{cm}^{-2}}$.

HITRAN¹ reports values of $S_{\tilde{\nu}}^N(T_{\text{ref}})$ at a reference temperature $T_{\text{ref}} = 296$ K, and they can be converted to other temperatures using equation (4)³².

$$S_{\tilde{\nu}}^N(T) = S_{\tilde{\nu}}^N(T_{\text{ref}}) \frac{Q_{\text{tot}}(T_{\text{ref}})}{Q_{\text{tot}}(T)} e^{-c_2 \tilde{E}_\ell (1/T - 1/T_{\text{ref}})} \left[\frac{1 - e^{c_2 \tilde{\nu}/T}}{1 - e^{c_2 \tilde{\nu}/T_{\text{ref}}}} \right] \quad (4)$$

where \tilde{E}_ℓ is the wavenumber corresponding to the energy of the lower level of the transition (also reported in HITRAN¹) and the function $Q(T)$ is the total internal partition sum (TIPS) that describes the statistical population of states at thermal equilibrium and which is discussed below. c_2 is a constant derived from other constants,

$$c_2 = \frac{hc}{k_B},$$

with units $\text{cm} \cdot \text{K}$. Here h is the Planck constant and c is the speed of light. Numerical evaluation of the direct partition function sum can require a heavy computational load,

however the result can be well approximated with a polynomial function, such as the one given in equation (5),³³ over a limited temperature range, with the understanding that the units of the analytically determined coefficients are inverse powers of T, such that the function remains dimensionless.

$$Q_{tot}(T) \approx -8.3088 + 1.4484T - 2.5946 \times 10^{-3}T^2 + 8.4612 \times 10^{-6}T^3, \quad (5)$$

We evaluated function (5) against other published empirical results³⁴ which showed a difference of less than 0.14% at temperatures near to 300 K. We also coded a direct numerical summation using molecular constants from Robert et al.³⁵ The results agreed with equ.(5) to better than 0.04% at the temperatures of interest in the present work, and also with the results of a more recent tabulation.³⁶ Details of these comparisons have been included in the Supplementary Data for this paper.

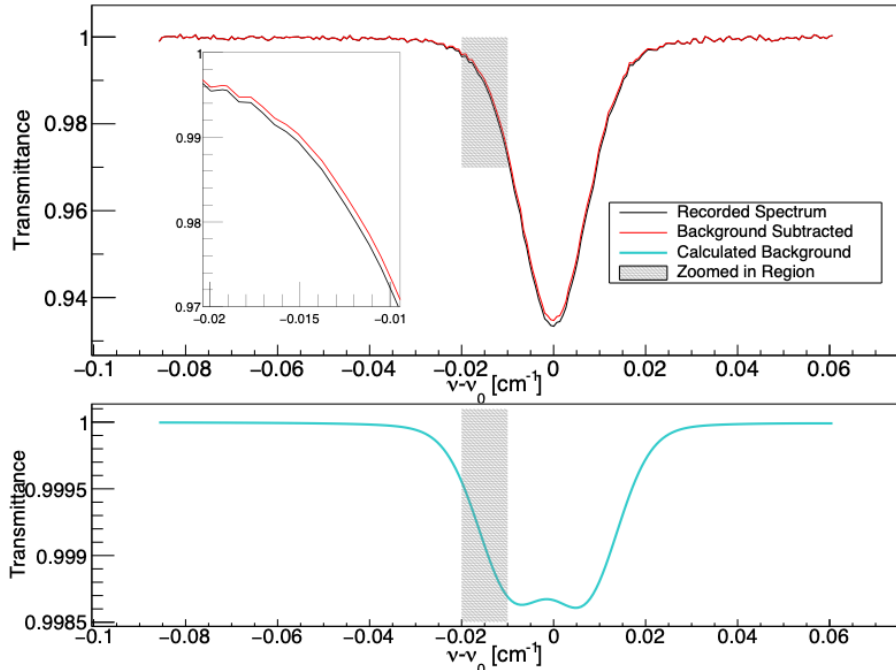
Equation (2) shows how the recorded data, $\frac{I_0}{I_t}(\tilde{\nu})$ is related to the molecular line shape, $g(\tilde{\nu} - \tilde{\nu}_0)$ which is an area normalized function. Since the IUPAC (International Union of Pure and Applied Chemistry) recommended²⁷ the adoption of the line shape proposed by Ngo et al.²⁶ in 2014, and named it the Hartmann-Tran Profile (HTP), it has increasingly become the lineshape model of choice in high resolution spectroscopy. A line profile fitting code written previously³⁷ was translated to Python. Fitting to the full set of parameters of the HTP requires extensive and very high signal-to-noise ratio (SNR) data, however the HTP has the advantage of being able to be reduced to several simpler line profile models²⁶ by nulling specific parameters. The Gaussian, Doppler-broadening, contribution for all profile models was calculated for the given temperature, and was not varied.³⁹

The commonly used Voigt Profile is obtained by eliminating all but the two most important contributions to the collisionally perturbed profile: the most probable collisional broadening (γ_0) and shift (δ_0). Adkins et al.²⁸ analyzed the effects of the smaller HTP parameters showing they are sensitive to different noise characteristics in the data and we experimented using different intermediate profile functions. The QSDVP gave the most reliable fit of the present data [see below] with fewest parameters varying. It contains the two parameters included in the VP, but also their speed-dependent variations, γ_2 and δ_2 . However, the pressure-dependent quadratic shift correction was not well determined in

preliminary fits to the data, which do not extend to sufficiently high pressure to determine it reliably, and δ_2 was fixed at zero for the data fitting discussed below.

B. Hotband corrections

FIG. 2. An example of the influence of background transitions near R(10), (1.091 kPa, 295.94 K). The calculated background line spectrum on the lower panel, unsymmetrically broadens the line of interest, as is seen in the zoomed region (highlighted).



The effects of weaker hot band and low abundance isotope lines lying close to the transitions of interest are not negligible. A background spectrum for a specific region, pressure and temperature was generated for each line by combining Voigt profiles using parameters from HITRAN¹, and included in the Supplementary Data for this paper. The frequency points from the actual data were used as the frequency variable to create the appropriate background function. This resulted in a one-to-one ratio of data points to background making background subtraction much simpler. It was a vital part of the data analysis since many weaker transitions lie near or underneath the transition of interest, and have absorptions of $\approx 1\%$ of the main line. Figure 2 shows the results for the R(10) transition where the neglect of the background transitions causes a strong distortion in the profile.

Several weak background lines in the data were not found in the HITRAN¹ list. They affected R(8) and R(12). Adjustments were made to empirically correct for these observed features by adding a VP feature. All the background lines included are detailed in the Supplementary Data for this paper.

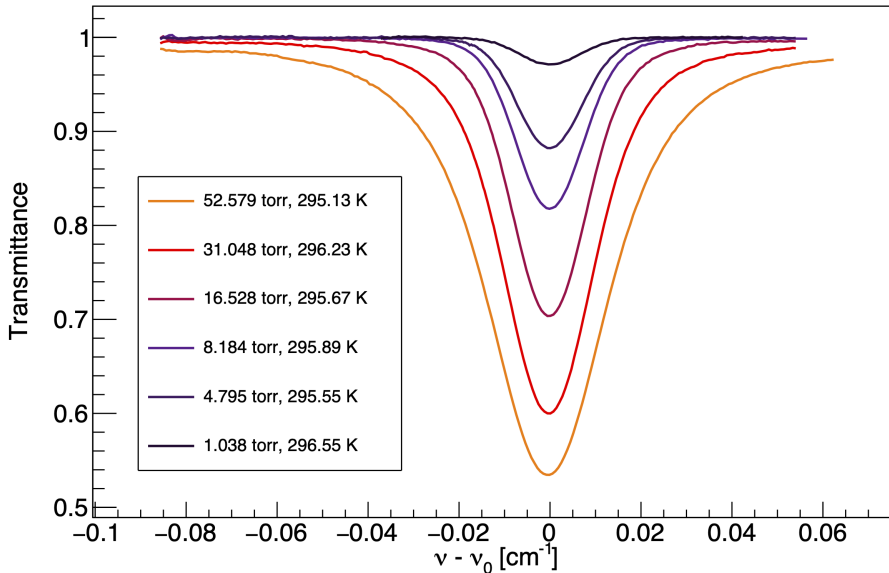
C. Baseline and amplitude fitting

As in our previous work,³⁷ small instrumental baseline deviations were accommodated into the profile fitting function. An initial set of parameters for a given transition together with hotband and weaker underlying features described above, were used to estimate a line profile and an apparent baseline function derived by subtracting it from the data. This was then fit to a second order polynomial to provide parameters to fit the baseline, as shown in the full fitting function used, Equation (6). The baseline of each transition at each pressure had to be individually fitted and the process was repeated after new line profile parameters were determined from the global fitting for a given transition, described below, until convergence.

$$\frac{I_0}{I_t}(\tilde{\nu} - \tilde{\nu}_0) = e^{-A \times \text{Amp} \times g(\tilde{\nu} - \tilde{\nu}_0)} + [b_0 + (\tilde{\nu} - \tilde{\nu}_0) \times b_1 + (\tilde{\nu} - \tilde{\nu}_0)^2 \times b_2] \quad (6)$$

The Hitran2016 linestrengths were found to closely reproduce the observed intensities, but to accommodate the small variations a dimensionless scaler multiplier, A, expected to be close to unity, was also introduced as a $S_{\tilde{\nu}}^N$ correction factor in Equation (6). The lowest-pressure scans, where the fixed Gaussian contribution to the line profiles dominates, were used in preliminary fitting to determine the amplitude corrections by floating the A multiplier alone. These multiplier values were then reevaluated over cycles of the multispectrum fit for each line until the final fit when all parameters were varied to yield the results in Table II.

FIG. 3. Absorbance data for R(9) at a series of pressures.



IV. RESULTS

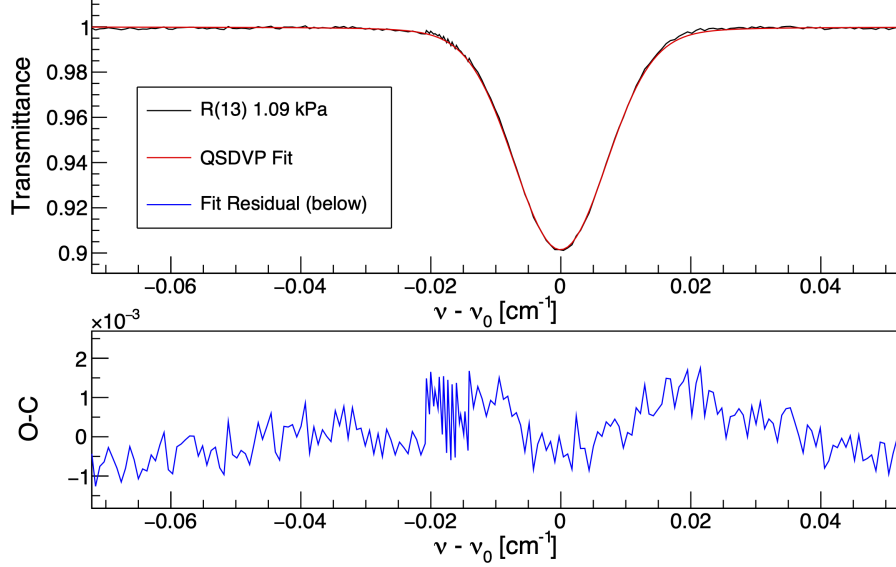
A. Introduction

An example of a sequence of pressure scans is shown in figure 3. Beyond the obvious pressure-broadening, a pressure dependent line frequency shift is also present, but it is small enough that it is difficult to see in the overview spectra. Averaging data points for one second provided an acceptable signal-to-noise ratio (SNR) for all pressures.

B. Line profile fitting

As a typical example, Figure 4 illustrates the results of fits to the data for R(13) at 1.091 kPa (8.184 torr). Overall, the QSDVP without δ_2 was found to be adequate to fit all the data. Table II presents the fitted parameters to the reduced QSDVP discussed above. The line strength multiplier values found are all slightly larger than, but within 2%, of unity and consistent with that seen in our previous work.³⁷ The results also agree with those from another recent measurement of the linestrengths in this band.⁴⁰ The Hitran2016 S_ν^N values for the line strengths are given in Table III. The differences between the newly measured and HITRAN linestrengths are factors of 10 larger than can be accounted for by the TIPS

FIG. 4. R(13) at 1.09 kPa (8.184 torr) and 294.4 K, fit to a QSDVP as detailed in the text, with the observed - calculated residual in the lower panel. The additional points around $nu - \nu_0$ are due to overlap between scans.



polynomial approximation, discussed in section III.

TABLE II. Results of the line profile modeling.

Line Label	γ_0	δ_0	γ_2	A
R(8)	0.15517 (40)	$-6.87 (23) \times 10^{-3}$	$2.261 (77) \times 10^{-2}$	1.0236 (10)
R(9)	0.15055 (16)	$-7.122 (90) \times 10^{-3}$	$2.121 (29) \times 10^{-2}$	1.01796 (39)
R(10)	0.14669 (39)	$-9.14 (22) \times 10^{-3}$	$2.059 (72) \times 10^{-2}$	1.0101 (11)
R(11)	0.14543 (15)	$-10.03 (87) \times 10^{-3}$	$1.643 (27) \times 10^{-2}$	1.00553 (42)
R(12)	0.14453 (41)	$-10.30 (24) \times 10^{-3}$	$1.832 (78) \times 10^{-2}$	1.0159 (12)
R(13)	0.14175 (17)	$-10.57 (10) \times 10^{-3}$	$1.947 (31) \times 10^{-2}$	1.01898 (46)

a. The S_ν^N multiplier is a dimensionless scaler.

b. All other parameters have units of $\text{cm}^{-1}/\text{atm}$.

c. The numbers in parenthesis are one standard deviation of the least squares fit in units of the last quoted significant figure. Systematic errors due mainly to background hotband lines probably add a factor or two or higher to these errors. See section IV C.

d. The quadratic shift, δ_2 could not be determined, see text for details.

There is a decreasing trend in the most probable self-broadening coefficient γ_0 with rotational quantum number, J , which is expected as rotational energy intervals increase. The results show reasonable agreement with published empirical fits^{42,43} of multiple published

TABLE III. Parameters used for line simulations, and initial fit parameters.

Line	Frequency ^a	$S_\nu^{N\ e, f}$	E_{low}^f	γ_0^b	$\delta_0^{c, d}$
R(7)	6574.361355	1.303×10^{-20}	65.887	0.162	-0.0071
R(8)	6576.481658	4.465×10^{-21}	84.710	0.158	-0.0077
R(9)	6578.575894	1.340×10^{-20}	105.885	0.154	-0.0082
R(10)	6580.644073	4.380×10^{-21}	129.411	0.150	-0.0088
R(11)	6582.686025	1.264×10^{-20}	155.289	0.147	-0.0093
R(12)	6584.701858	3.977×10^{-21}	183.517	0.144	-0.0098
R(13)	6586.691493	1.107×10^{-20}	214.096	0.141	-0.0103
R(14)	6588.654889	3.369×10^{-21}	247.024	0.138	-0.0108

a. In cm^{-1} , from reference⁴¹

b. References^{23,42,43}

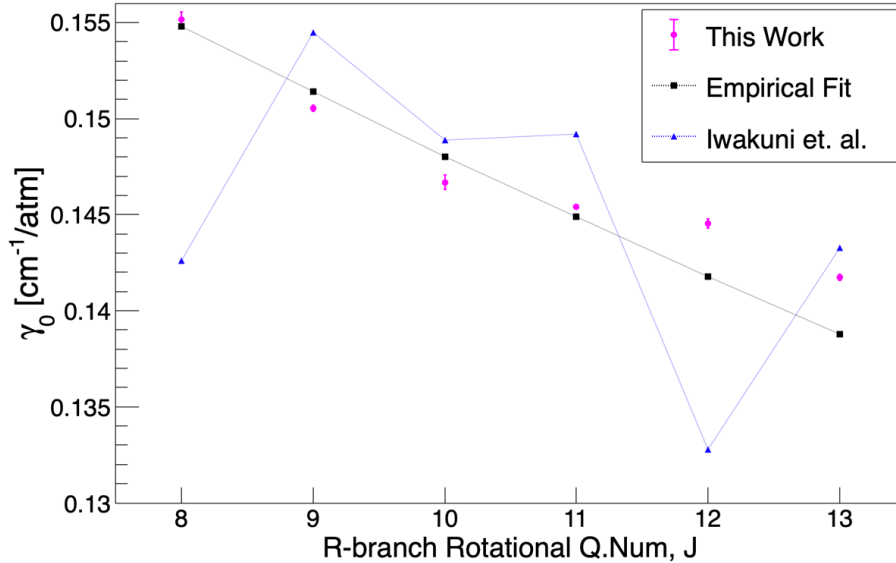
c. From Iwakuni et al.⁶

d. $\gamma_2 = 0.0212$ & $\delta_2 = -0.00132$ assumed for all lines.³⁷.

e. Line strength factor¹ in units of $\text{molecule}^{-1}.\text{cm}$ for 296 K.

f. In cm^{-1} , from reference¹

FIG. 5. Most probable speed-dependent (γ_0) and Voigt (γ) self pressure-broadening parameters comparisons, with statistical errors for the lines R(8)-R(13) in units of $\text{cm}^{-1}\text{atm}^{-1}$. Empirical Fit from^{23,42,43}, and Iwakuni et al.²⁵.



results to smooth functional forms, and the HITRAN database, as is illustrated in Figure 5. Importantly, there is no evidence for the kind of systematic reduction in the average self-broadening parameter for *para*- lines compared to *ortho*- ones reported by Iwakuni et al. and also shown in this figure. This disagreement is most likely due to the reasons outlined by Hartmann and Tran,²⁴ and is investigated more thoroughly in subsection IV D below.

C. Estimates of Systematic Errors

It is well known³⁷ that the statistical parameter uncertainties derived from global fits of high precision data such as performed here, tend to be underestimates of the actual values. The baseline noise in the data is well represented by a Gaussian distribution with amplitude of approximately ± 0.0005 in transmittance units but errors deriving from uncertainties in the pressure and temperature measurements and inaccurate accounting for weak background absorptions can cause much larger errors.

Systematic errors caused by inaccurate pressure measurements were estimated in a Monte Carlo type analysis described previously.³⁷ A synthetic dataset for a single rotational transition (R(9) was selected) was generated using the parameters in Table II. The pressures were randomly modified following a Gaussian distribution with a width determined by a fixed percentage of the measured pressure corresponding to a value near to the pressure gauge manufacturer's specification, and the global fit performed. This was repeated 256 times to generate a distribution of parameter values whose standard deviation was determined. The process was repeated for greater and smaller assumed pressure error amplitudes.

For pressure measurement errors at the level of the specification of the gauge head, the parameter errors were similar to the statistical standard deviations quoted in Table II. As the assumed pressure error is increased, parameter standard deviations increased approximately linearly, with slopes of 0.1 for γ_0 , 0.01 for δ_0 0.05 for γ_2 and 0.1 for the amplitude multiplier, A. That is, for example, a 1% increase in pressure uncertainties results in a 0.1% increase in the γ_0 error estimate. Systematic errors due to any reasonable assumed uncertainty in temperature measurements are negligible.

The largest errors derive from inaccuracies in the treatment of weak background lines and they were investigated by adding a background line with a linestrength fixed at a (small) fraction of the main line at various frequency offsets from the center of the main line. Modeling showed that the maximum strength of a background feature that would be unrecognized was at the level of approximately 0.001 times the S_{ν}^N of the main line. For R(9) this led to a variation in γ_0 of $\pm 0.0003 \text{ cm}^{-1} \text{ atm}^{-1}$, *i.e.* about twice the statistical uncertainty

in table II. Results for γ_2 , δ_0 , and A were ± 0.02 , ± 0.03 and ± 0.00005 respectively, that is all larger than their statistical uncertainties. Similar relative increases can be expected in the parameter uncertainties for the other lines. The VP γ assumed for the background lines is also a concern, since they are typically not well measured and values assumed by extrapolation from sparse data. Modeling showed that a change of $0.01 \text{ cm}^{-1}\text{atm}^{-1}$ in the assumed broadening coefficient for some background lines caused changes to the γ_0 values given in table II outside the statistical uncertainties.

D. Modeling VP fits to experimental data in the low transmittance regime

Hartmann and Tran²⁴ claimed that the VP is an unreliable line shape model when applied to transmission spectral data recorded under conditions when peak absorbances approach unity, especially at low pressures. It is noticeable that in Figure 1 of the Iwakuni et al. rebuttal²⁵ of this criticism which showed data for the R(9) transition, the line center is close to 100% absorbing under nearly all their experimental conditions. To simulate the data and investigate the parameter space, we have modified the MATLAB code developed previously.³⁷ This simulates a line in a transmittance spectrum using a HTP model, then attempts to fit it to a simplified model.

Line profiles in transmission for the R-branch transitions with $J=7$ to $J=14$ were calculated at the level of the QSDVP model for the exact experimental conditions used by Iwakuni et al.^{6,25} The profile model includes the broadening and shift coefficients (γ_0 and δ_0) for the most probable speed, and their speed-dependent corrections (γ_2 and δ_2). The relevant parameters are summarized in Table III. The Gaussian (Doppler) contribution was again fixed at the expected gas kinetic value. The line strengths were assumed to be those in the HITRAN 2016 database.¹ To these calculated line profiles, random Gaussian noise with an amplitude of 0.008 transmittance units, as estimated from the noise in the observed-calculated residuals in figure 1 of Iwakuni et al.,²⁵ was added. These noisy simulations were then least-squares fitted to a Voigt profile model with the speed-dependent profile parameters (γ_2 and δ_2) fixed at zero. Two examples of the simulated line profiles and fits to the Voigt profile for R(9) are shown in Figure 6.

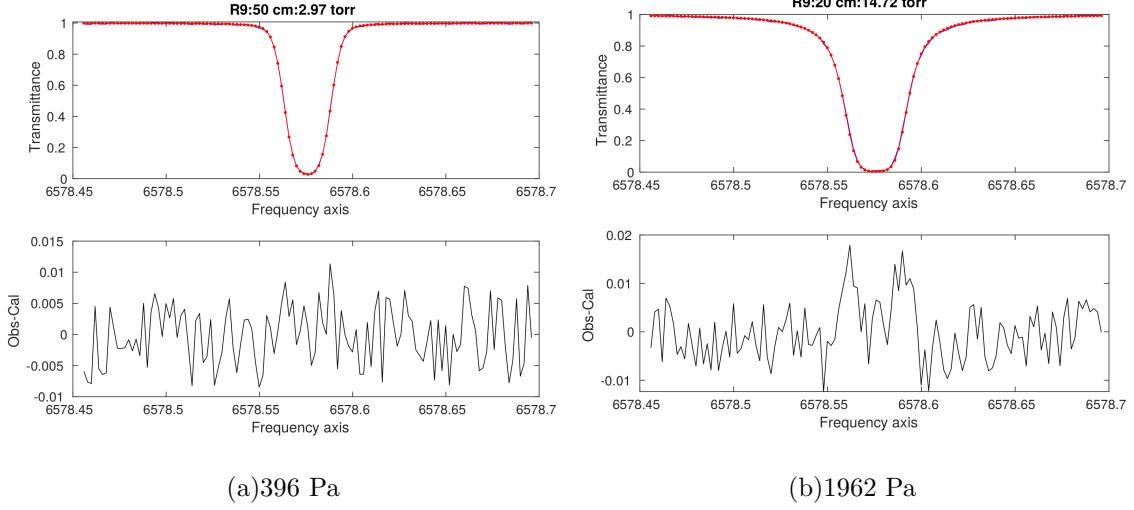


FIG. 6. Simulated QSDV profiles for R(9) at 396 Pa and 1962 Pa and observed - calculated residuals from fits to a Voigt profile model. Red dots in the spectra are the simulations and the line the fit to a Voigt profile.

We found the HITRAN linestrengths always predicted a larger absorption at line center than shown in figure 1 of Iwakuni et al²⁵ as is clear from the examples in figure (6). To reproduce precisely the published²⁵ strengths the linestrength factor had to be reduced by approximately 20%. However, except where explicitly discussed below, in the simulations we have retained the HITRAN values for S_v^N given in table III. In the spectral simulations shown by Iwakuni et al., it is not stated whether the absolute intensities are fixed or allowed to vary to fit the data. The effects of reducing the peak absorptions are investigated below. Note the residuals from the simulation of the higher pressure line in figure (6) show evidence for the M-shaped residual that is indicative of the neglect of collisional narrowing in the Voigt model,

Simulations and fits were carried out as described above and the effective γ and δ broadening and shift parameters in the Voigt approximation determined by linear fits of the Lorentzian broadening and pressure shift at the observed pressures. In these fits, the smaller parameters in the QSDV profile, *i.e.* γ_2 and δ_2 , were set to zero. In order to generate a statistical sample, the process was repeated for (typically) 256 times with different random Gaussian noise applied to the synthetic line shape at each cycle. The standard deviations of the multiple determinations of γ_0 and δ_0 were computed to estimate the errors in the

determined coefficients. The results are summarized in the two plots in figure 7.

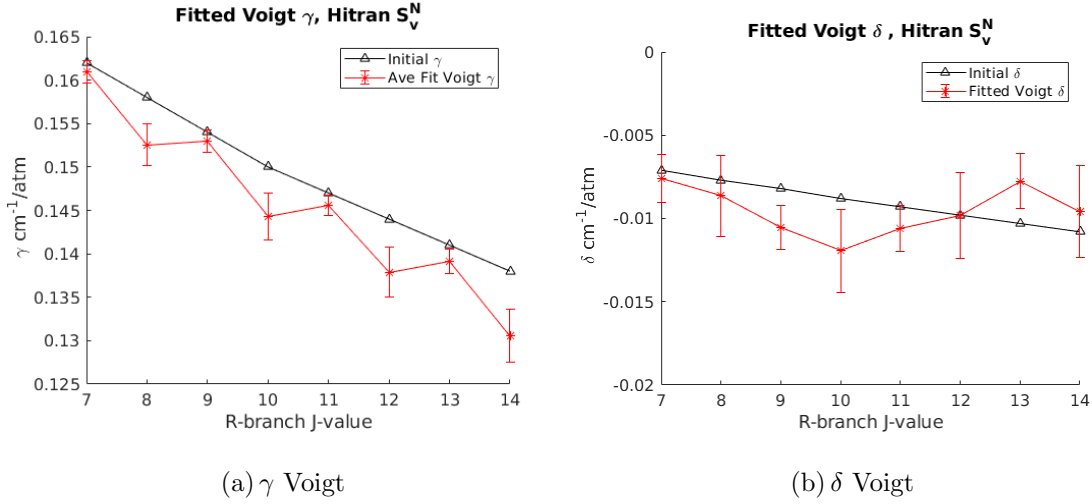


FIG. 7. Fits of the Voigt broadening and shift coefficients to the simulated noisy data in transmission with γ_2 and δ_2 fixed at zero for all lines.

The most important result in Figure 7 is the sawtooth-like behavior of the broadening coefficient. The *ortho*- lines are found to have an apparently larger broadening coefficient than the *para*- lines, exactly as found in the original report. This occurs even when the simulations were generated assuming a smoothly varying broadening coefficient. The pressure shift coefficient is not subject to the same systematic variation and the fitted values are more or less symmetric about the values used for the simulated data.

Studying the behavior further, several factors were investigated and the details are available as supplementary material for this paper. Briefly the fitting was repeated with γ_2 fixed at the non-zero value used in the model simulations. The values determined for the self-broadening coefficient now coincide with those used in the simulations, there was no evidence for any systematic *ortho*- *para*- variation. If γ_2 values of one-half of those used in the simulations were chosen, the amplitude of the variation in the self-broadening coefficients determined returned, but at reduced amplitude.

In order to assess changes to the results as the peak line absorptions decreased, calculations were repeated for the line strength coefficients (S_V^N) arbitrarily multiplied by factors

of 0.8 and 0.6. As the absorption strength decreases, the *ortho-para*- variation with J decreases and the average value of the broadening coefficient determined also decreases, reflecting efforts to accommodate the collisional narrowing in the fitting. We therefore conclude that the systematic variation in γ is indeed an artifact arising due to the use of the inaccurate Voigt profile model in fitting the data.

Hartmann and Tran²⁴ asserted the apparent *ortho-para*- variations go away when the data is treated in the absorbance representation, so the simulation code was modified to work in this representation, that is the negative log base 10 of the transmittance signals. As shown and discussed in detail in the supplementary material, there is a clear distinction between the results in the two representations. In the absorbance representation, there is no indication of the oscillation in the variation of the values of γ determined from fits of the simulated data to the approximate Voigt profile model that was seen when fitting to transmittance data. The absolute values of the coefficient are systematically smaller than the actual values, but again this is the well-known artifact of fitting to a Voigt profile when collisional narrowing is present. In order to minimize the deviations, a narrower profile is needed, so the broadening parameter determined is smaller. Iwakuni et al.²⁵ modeled this effect by allowing for an, unphysical, narrower Doppler (Gaussian) contribution, to the Voigt convolution.

E. Conclusions and Summary

We have measured rotation-vibration lines with roational quantum numbers between 8 and 13 in the R-branch of the $\nu_1 + \nu_3$ band in acetylene using an OFC-locked ECLD spectrometer. Our measurements lacked any alternation in the pressure self-broadening coefficient, which did not agree with the report of Iwakuni et al.⁶. By detailed modeling of the results of Iwakuni et al. we showed that the alternation was an artifact due to the use of the Voigt profile that neglects collisional narrowing in transmission data, in a strongly absorbing regime.

V. SUPPLEMENTARY MATERIAL

List of items included in supplementary data for this paper.

1. Hot band and low abundance isotope lines included in the modeling of the experimental data.
2. Details of the simulations used for modeling the data of Iwakuni et al^{6,25} with a VP.
3. Matlab codes for calculating the Internal Partition Function for acetylene.
4. Details of Python codes for data analysis and links to Gitlab repositories.

VI. DATA AVAILABILITY STATEMENT

The experimental data that supports the findings of this study is available from the corresponding author upon reasonable request. The data analysis programs are available in the Gitlab repository as detailed in the Appendix and Supplementary Material for this paper.

VII. ACKNOWLEDGEMENTS

This work was supported by the U.S. Department of Energy, Office of Science, Division of Chemical Sciences, Geosciences and Biosciences within the Office of Basic Energy Sciences, under Award Number DE-SC0018950. This research made use of the MINUIT algorithm⁴⁴ via the iminuit⁴⁵ Python interface. We are most grateful for discussions and correspondence with Professors Sasada (Keio University, Japan) and Hartmann (IPLS, Ecole Polytechnique, France) during the course of this work.

VIII. APPENDIX

Copies of the programs described below are available on a GitLab repository, <https://gitlab.com/Eiceman/pbroadgfit> 10.5281/zenodo.3672083

REFERENCES

- ¹I. Gordon, L. Rothman, C. Hill, R. Kochanov, Y. Tan, P. Bernath, M. Birk, V. Boudon, A. Campargue, K. Chance, B. Drouin, J.-M. Flaud, R. Gamache, J. Hodges, D. Jacquemart, V. Perevalov, A. Perrin, K. Shine, M.-A. Smith, J. Tennyson, G. Toon, H. Tran, V. Tyuterev, A. Barbe, A. Császár, V. Devi, T. Furtenbacher, J. Harrison, J.-M. Hartmann, A. Jolly, T. Johnson, T. Karman, I. Kleiner, A. Kyuberis, J. Loos, O. Lyulin, S. Massie, S. Mikhailenko, N. Moazzen-Ahmadi, H. Müller, O. Naumenko, A. Nikitin, O. Polyansky, M. Rey, M. Rotger, S. Sharpe, K. Sung, E. Starikova, S. Tashkun, J. V. Auwera, G. Wagner, J. Wilzewski, P. Wcisło, S. Yu, and E. Zak, “The HITRAN2016 molecular spectroscopic database,” *J. Quant. Spectrosc. Rad. Transf.* **203**, 3 – 69 (2017).
- ²J. Hartmann, C. Boulet, and D. Robert, *Collisional Effects on Molecular Spectra* (Elsevier, 2008).
- ³J.-M. Hartmann, H. Tran, N. H. Ngo, X. Landsheere, P. Chelin, Y. Lu, A.-W. Liu, S.-M. Hu, L. Gianfrani, G. Casa, A. Castrillo, M. Lepère, Q. Delière, M. Dhyne, and L. Fissiaux, “Ab-initio calculations of the spectral shapes of CO₂ isolated lines including non-Voigt effects and comparisons with experiments,” *Phys. Rev. A* **87**, 013403 (2013).
- ⁴J.-M. Hartmann, H. Tran, R. Armante, C. Boulet, A. Campargue, F. Forget, L. Gianfrani, I. Gordon, S. Guerlet, M. Gustafsson, J. T. Hodges, S. Kassi, D. Lisak, F. Thibault, and G. C. Toon, “Recent advances in collisional effects on spectra of molecular gases and their practical consequences,” *J. Quant. Spectrosc. Rad. Transf.* **213**, 178 – 227 (2018).
- ⁵H. T. Nguyen, N. H. Ngo, and H. Tran, “Line-shape parameters and their temperature dependences predicted from molecular dynamics simulations for O₂ and air-broadened CO₂ lines,” *J. Quant. Spectrosc. Rad. Transf.* **242**, 106729 (2020).
- ⁶K. Iwakuni, S. Okubo, K. M. Yamada, A. Onae, F.-L. Hong, and H. Sasada, “Ortho-para dependent pressure effects observed in the near infrared band of acetylene by dual-comb spectroscopy,” *Phys. Rev. Letts.* **117**, 143902(5) (2016).
- ⁷T. Udem, R. Holzwarth, and T. W. Hänsch, “Optical frequency metrology,” *Nature* **416**, 233–237 (2002).
- ⁸D. J. Jones, “Carrier-Envelope Phase Control of Femtosecond Mode-Locked Lasers and Direct Optical Frequency Synthesis,” *Science* **288**, 635–639 (2000).
- ⁹S. A. Diddams, “An optical clock based on a single trapped ¹⁹⁹Hg⁺ ion,” *Science* **293**, 825–828 (2001).
- ¹⁰B. R. Washburn, S. A. Diddams, N. R. Newbury, J. W. Nicholson, M. F. Yan, and C. G. Jørgensen, “Phase-locked, erbium-fiber-laser-based frequency comb in the near infrared,” *Optics Letts.* **29**, 250 (2004).

- ¹¹S. A. Diddams, L. Hollberg, and V. Mbele, “Molecular fingerprinting with the resolved modes of a femtosecond laser frequency comb,” *Nature* **445**, 627–630 (2007).
- ¹²C. McRaven, M. Cich, G. Lopez, T. J. Sears, D. Hurtmans, and A. Mantz, “Frequency comb-referenced measurements of self- and nitrogen-broadening in the $\nu_1 + \nu_3$ band of acetylene,” *J. Molec. Spectrosc.* **266**, 43–51 (2011).
- ¹³P. W. Anderson, “Pressure broadening in the microwave and infra-red regions,” *Phys. Rev.* **76**, 647–661 (1949).
- ¹⁴R. Keijser, J. Lombardi, K. V. den Hout, B. Sanctuary, and H. Knaap, “The pressure broadening of the rotational Raman lines of hydrogen isotopes,” *Physica* **76**, 585 – 608 (1974).
- ¹⁵K. V. D. Hout, P. Hermans, E. Mazur, and H. Knaap, “The broadening and shift of the rotational raman lines for hydrogen isotopes at low temperatures,” *Physica A: Statistical Mechanics and its Applications* **104**, 509 – 547 (1980).
- ¹⁶L. A. Rahn, R. L. Farrow, and G. J. Rosasco, “Measurement of the self-broadening of the H_2 Q(0–5) Raman transitions from 295 to 1000 K,” *Phys. Rev. A* **43**, 6075–6088 (1991).
- ¹⁷C. Gray, “Pressure-broadening of the rotational raman lines of hcl,” *Chem. Phys. Letts.* **8**, 527 – 528 (1971).
- ¹⁸N. Rich and H. Welsh, “Measurement of the pressure broadening of the rotational Raman lines of HCl,” *Chem. Phys. Letts.* **11**, 292 – 293 (1971).
- ¹⁹D. Fabre, G. Widenlocher, and H. Vu, “Etude experimentale de l’elargissement par la pression des raies de rotation du spectre raman de l’acide chlorhydrique,” *Optics Communications* **4**, 421 – 424 (1972).
- ²⁰A. M. Smith, K. K. Lehmann, and W. Klemperer, “The intensity and self-broadening of overtone transitions in HCN,” *J. Chem. Phys.* **85**, 4958–4965 (1986), <https://doi.org/10.1063/1.451734>.
- ²¹W. Swann and S. Gilbert, “Line centers, pressure shift, and pressure broadening of 1530-1560 nm hydrogen cyanide wavelength calibration lines,” *J. Opt. Soc. Amer. B-Opt. Phys.* **22**, 1749–1756 (2005).
- ²²J. Bouanich, C. Boulet, A. Predoi-Cross, S. Sharpe, R. Sams, M. Smith, C. Rinsland, D. Benner, and V. Devi, “A multispectrum analysis of the ν_2 band of (HCN)-C-12-N-14: Part II. Theoretical calculations of self-broadening, self-induced shifts, and their temperature dependences,” *J. Molec. Spectrosc.* **231**, 85–95 (2005).
- ²³K. K. Lehmann, “Influence of resonant collisions on the self-broadening of acetylene,” *J. Chem. Phys.* **146** (2017), 10.1063/1.4977726.

- ²⁴J.-M. Hartmann and H. Tran, “Comment on “ortho-para-dependent pressure effects observed in the near infrared band of acetylene by dual-comb spectroscopy”,” *Phys. Rev. Lett.* **119**, 069401 (2017).
- ²⁵K. Iwakuni, S. Okubo, K. M. T. Yamada, H. Inaba, A. Onae, F.-L. Hong, and H. Sasada, “Iwakuni et al. reply:,” *Phys. Rev. Lett.* **119**, 069402 (2017).
- ²⁶N. H. Ngo, H. Tran, and J. M. Hartmann, “An isolated line-shape model to go beyond the Voigt profile in spectroscopic databases and radiative transfer codes,” *J. Quant. Spectrosc. Rad. Transf.* **129**, 89–100 (2013).
- ²⁷J. Tennyson, P. F. Bernath, A. Campargue, A. G. Császár, L. Daumont, R. R. Gamache, J. T. Hodges, D. Lisak, O. V. Naumenko, L. S. Rothman, H. Tran, N. F. Zobov, J. Buldyreva, C. D. Boone, M. D. De Vizia, L. Gianfrani, J.-M. Hartmann, R. McPheat, D. Weidmann, J. Murray, N. H. Ngo, and O. L. Polyansky, “Recommended isolated-line profile for representing high-resolution spectroscopic transitions (IUPAC Technical Report),” *Pure and Applied Chemistry* **86**, 1931–1943 (2014).
- ²⁸E. Adkins and J. Hodges, “Numerical evaluation of Hartmann-Tran line profile use in synthetic, noisy spectra,” in *Proceedings of the 74th International Symposium on Molecular Spectroscopy* (University of Illinois at Urbana-Champaign, Urbana, Illinois USA, 2019) pp. 1–1.
- ²⁹M. J. Cich, D. Forthomme, C. P. McRaven, G. V. Lopez, G. E. Hall, T. J. Sears, and A. W. Mantz, “Temperature-dependent, nitrogen-perturbed line shape measurements in the $\nu_1 + \nu_3$ band of acetylene using a diode laser referenced to a frequency comb,” *J. Phys. Chem. A* **117**, 13908–13918 (2013), <http://dx.doi.org/10.1021/jp408960e>.
- ³⁰C. McRaven, M. Cich, G. Lopez, T. J. Sears, D. Hurtmans, and A. Mantz, “Frequency comb-referenced measurements of self- and nitrogen-broadening in the $\nu_1 + \nu_3$ band of acetylene,” *J. Molec. Spectrosc.* **266**, 43 – 51 (2011).
- ³¹R. Holzwarth, T. Udem, T. W. Hänsch, J. C. Knight, W. J. Wadsworth, and P. S. J. Russell, “Optical frequency synthesizer for precision spectroscopy,” *Phys. Rev. Letts.* **85**, 2264–2267 (2000).
- ³²M. Šimečková, D. Jacquemart, L. S. Rothman, R. R. Gamache, and A. Goldman, “Einstein A-coefficients and statistical weights for molecular absorption transitions in the hitran database,” *Journal of Quant. Spectrosc. Rad. Transf.* **98**, 130–155 (2006).
- ³³R. Gamache, S. Kennedy, R. Hawkins, and L. Rothman, “Total internal partition sums for molecules in the terrestrial atmosphere,” *J. Molec. Struct.* **517**, 407–425 (2000).
- ³⁴B. Amyay, A. Fayt, and M. Herman, “Accurate partition function for acetylene, $^{12}\text{C}_2\text{H}_2$, and related thermodynamical quantities,” *J. Chem. Phys.* **135**, 234305 (2011), <https://doi.org/10.1063/1.3664626>.

- ³⁵S. Robert, M. Herman, J. V. Auwera, G. D. Lonardo, L. Fusina, G. Blanquet, M. Lepere, and A. Fayt, “The bending vibrations in $^{12}\text{C}_2\text{H}_2$: global vibration–rotation analysis,” *Molec. Phys.* **105**, 559–568 (2007), <https://doi.org/10.1080/00268970601099261>.
- ³⁶R. R. Gamache, C. Roller, E. Lopes, I. E. Gordon, L. S. Rothman, O. L. Polyansky, N. F. Zobov, A. A. Kyuberis, J. Tennyson, S. N. Yurchenko, A. G. Császár, T. Furtenbacher, X. Huang, D. W. Schwenke, T. J. Lee, B. J. Drouin, S. A. Tashkun, V. I. Perevalov, and R. V. Kochanov, “Total internal partition sums for 166 isotopologues of 51 molecules important in planetary atmospheres Application to HITRAN2016 and beyond,” *J. Quant. Spectrosc. Rad. Transf.* **203**, 70 – 87 (2017), HITRAN2016 Special Issue.
- ³⁷D. Forthomme, M. J. Cich, S. Twagirayezu, G. E. Hall, and T. J. Sears, “Application of the Hartmann–Tran profile to precise experimental data sets of $^{12}\text{C}_2\text{H}_2$,” *J. Quant. Spectrosc. Rad. Transf.* **165**, 28–37 (2015).
- ³⁸S. G. Johnson, “Faddeeva w function implementation. http://ab-initio.mit.edu/wiki/index.php/Faddeeva_Package,” (2009–).
- ³⁹C. H. Townes and A. L. Schawlow, *Microwave Spectroscopy* (Dover Publications, New York, 1975).
- ⁴⁰S. Okubo, K. Iwakuni, K. M. Yamada, H. Inaba, A. Onae, F.-L. Hong, and H. Sasada, “Transition dipole-moment of the $\nu_1 + \nu_3$ band of acetylene measured with dual-comb Fourier-transform spectroscopy,” *J. Molec. Spectrosc.* **341**, 10 – 16 (2017).
- ⁴¹A. A. Madej, A. J. Alcock, A. Czajkowski, J. E. Bernard, and S. Chepurov, “Accurate absolute reference frequencies from 1511 to 1545 nm of the $\nu_1 + \nu_3$ band of $^{12}\text{C}_2\text{H}_2$ determined with laser frequency comb interval measurements,” *J. Opt. Soc. Am. B* **23**, 2200–2208 (2006).
- ⁴²M. Kusaba and J. Henningsen, “The $\nu_1 + \nu_3$ and the $\nu_1 + \nu_2 + \nu_4^1 + \nu_5^{-1}$ combination bands of $^{13}\text{C}_2\text{H}_2$, linestrengths, broadening parameters and pressure shifts,” *J. Molec. Spectrosc.* **209**, 216–227 (2001).
- ⁴³D. Jacquemart, J.-Y. Mandin, V. Dana, L. Regalia-Jarlot, J. J. Plateaux, D. Decatoire, and L. S. Rothman, “The spectrum of acetylene in the 5- μm region from new line parameter measurements,” *J. Quant. Spectrosc. Rad. Transf.* **76**, 237–267 (2003).
- ⁴⁴F. James and M. Roos, “Minuit – a system for function minimization and analysis of the parameter errors and correlations,” *Computer Physics Communications* **10**, 343–367 (1975).
- ⁴⁵The iMinuit Team, “iMinuit – A Python interface to Minuit. <https://github.com/scikit-hep/iminuit>,” (2013–).